Journal of Nuclear Materials 378 (2008) 282–290

Contents lists available at ScienceDirect

Journal of Nuclear Materials

journal homepage: www.elsevier.com/locate/jnucmat

# Influence of different chemical elements on irradiation-induced hardening embrittlement of RPV steels

M. Lambrecht *, L. Malerba, A. Almazouzi

*SCK•CEN, Nuclear Materials Sciences Institute, Boeretang 200, B-2400 Mol, Belgium*

ARTICLE INFO

*Article history:*
Received 9 June 2008
Accepted 10 June 2008

*PACS:*
28.52.Fa
62.20.−x
78.70.Bj

ABSTRACT

Fe–Cu binary alloys are often used to mimic the behaviour of reactor pressure vessel steels. Their study allows identifying some of the defects responsible for irradiation-induced hardening. But recently the influence of manganese and nickel in low-Cu steels has been found to be important as well. In contrast with existing models found in the literature, which predict that hardening saturates after a certain dose, Fe alloys containing nickel and manganese irradiated in a material test reactor (BR2) show a continuous increase of hardening, up to doses equivalent to about 40 years of operation. Considerations based on positron annihilation spectroscopy analyses suggest that the main objects causing hardening in Cu-free alloys are most probably self-interstitial clusters decorated with manganese. In low-Cu reactor pressure vessel steels and in Fe–CuMnNi alloys, the main effect is still due to Cu-rich precipitates at low doses, but the role of manganese-related features becomes pre-dominant at higher doses.

© 2008 Elsevier B.V. All rights reserved.

## 1. Introduction

The irradiation-induced hardening and embrittlement of reactor pressure vessel (RPV) steels are a great concern for nuclear power plant (NPP) life assessment. For the sake of their preservation, NPPs have been the subject of extensive investigations for many years [1]. It was observed that the materials used for the reactor vessels are prone to embrittle due to irradiation. However, the real nature of the radiation damage responsible for this embrittlement and its evolution with dose remain elusive and still require close examination.

The current surveillance procedure of irradiated pressure vessels is based on Charpy-V tests. Capsules are usually installed at the inner shell of the reactor at the beginning of its life cycle and are extracted to perform tests according to a predefined schedule. However, in most NPPs these capsules are getting exhausted, because their planned lifetime is reaching its end. To extend their lifetime, reliable predictive models are urgently needed, based simultaneously on experiments and computer simulation. The detailed study of defect formation under neutron irradiation, their evolution and their thermal stability are of paramount importance for the identification of the hardening mechanisms that the models should include.

Presently, the progress achieved in advanced experimental techniques, such as, for example, transmission electron microscopy (TEM), positron annihilation spectroscopy (PAS), internal friction (IF), tomographic atom probe (TAP) and small angle neutron scattering (SANS), enables a detailed investigation of the nano-features induced by irradiation in RPV steels to be performed [2]. Within the PERFECT project, these techniques have been used in a combined fashion to investigate the same materials (the 'REVE'-experiments [3]). For the present work, the experiments conducted by PAS in this PERFECT framework were used to interpret the corresponding hardening results that were obtained by tensile tests, with the support of a few computer-modelling results and theoretical considerations. The overall analysis, based on the combination of all results from all mentioned techniques, will be published in the near future.

Irradiation-induced embrittlement in RPV steels is conventionally ascribed to three main causes [2,4]: precipitation, matrix-damage and grain boundary segregation. While precipitation and segregation have been profoundly studied [4], it is still unclear what the nature and the main mechanisms of the formation of matrix damage are. Small vacancy and interstitial clusters are well known to be produced directly in displacement cascades in Fe [5,6]. These clusters then aggregate to form larger defects, such as nano-voids and self-interstitial loops. At the same time, solute atoms may diffuse to these clusters, giving rise to large, complex defect-solute configurations. But which solutes and how and why they stabilize clusters is still a debated matter.

PAS gives valuable information on irradiation-induced vacancy-type defects [7–10]. In this technique, the positron is applied as a probe. As anti-particle of the electron, the positron is trapped by defects with a different electron density than the bulk-material, such as vacancies, vacancy clusters, interfaces, second phase

* Corresponding author. Tel.: +32 14 33 30 89; fax: +32 14 32 12 16.
*E-mail address:* Marlies.Lambrecht@SCKCEN.BE (M. Lambrecht).

0022-3115/$ - see front matter © 2008 Elsevier B.V. All rights reserved.
doi:10.1016/j.jnucmat.2008.06.030

particles, dislocations, etc. [11]. The annihilation characteristics in the neighbourhood of defects are different when compared to defect-free materials. Moreover, due to the difference in positron affinity of the different atomic species, positrons annihilate with another probability in the precipitates as compared to the bulk-material [12]. The power of PAS lies in its 'self-seeking' and non-destructive nature, which gives the possibility to find very small defects (>0.1 nm) even in very low concentrations (>1 ppm). It is used in many different fields of material science, for instance to characterize building materials (e.g. cement [13]), polymers [14,15], semiconductor-based systems for information technology [16], as well as for the characterisation of nuclear materials [7–9].

Significant progress in revealing potential vacancy clusters has been made by PAS during the past decades [17–21]. The focus is now being put on the chemical surroundings of the clusters that are sensitive to positrons, to obtain a better understanding of the nature of the matrix damage. Positrons are indeed sensitive to precipitate–matrix interfaces. Therefore, a substantial effort is being re-deployed to use this technique to identify the ultimate causes of hardening and embrittlement in RPV steels, particularly with a view to developing physically based models. In this paper, the results obtained from PAS investigations of different neutron-irradiated Fe and Fe–Cu alloys as well as of Fe–MnNi and Fe–CuMnNi alloys, are described and discussed. The results are then correlated to the irradiation-induced hardening data obtained from the same samples [22]. For the sake of comparison, also a Western type RPV steel was examined.

## 2. Materials and irradiation conditions

Starting from electrolytic iron, seven different model alloys were fabricated, with growing chemical complexity between two extremes, pure iron and a real RPV steel. The materials were prepared using argon-arc melting and zone refinement methods. The resulting ingots were cold-worked after austenisation tempering. A final heat treatment at 1075 K for 1 h was performed to release the stresses and to get well re-crystallized materials. This was followed by water quenching.

Table 1 lists the results of the chemical composition of the alloys. The analyses were performed by induced coupled plasma spectroscopy for the metallic elements, while C and N were measured using the combustion technique. The carbon concentration of all alloys is below the detection limit of these techniques. However, based on the appearance of the Snoeck peak in internal friction measurements, it can be deduced that the C content is much less than 20 ppm for all model-alloys, except for the Fe–C alloy. In the latter, the concentration of C should be at least 50 ppm.

On top of this, Table 2 gives the average grain size and the dislocation density before irradiation of each alloy, obtained by conventional metallography and the TEM, respectively. While the grain size decreases slightly with increasing alloy complexity, the dislocation density is almost the same in all alloys.

All the materials have been irradiated in the test reactor BR2 at SCK•CEN, to different doses. The temperature and the pressure were maintained constant during irradiation between 290 °C and 295 °C and at 150 bar, respectively. In this paper, the entire set of specimens irradiated up to 0.1 dpa ($\sim 7 \times 10^{19}$ n/cm$^2$ at a neutron flux of $8.6 \pm 0.5 \times 10^{13}$ n/cm$^2$/s, with $E_n > 1$ MeV) is taken into consideration with the aim to reveal the effect of each chemical element on the development of matrix damage and its influence on the material hardening. This irradiation dose corresponds to about 40 years of operation, i.e. the planned end-of-life of most NPPs around the world.

## 3. Measurement and analysis

Positron lifetime (PLT) and coincidence Doppler broadening (CDB) spectroscopy, both available in the hot cell laboratory of SCK•CEN, have been used in a complementary way. PLT measurements give information on the electronic structure of the material at the place of annihilation, while CDB spectroscopy is used to measure the positron affinity of the atoms in the neighbourhood of the annihilation site. These results have been correlated with the mechanical properties that were obtained from tensile tests, measured before and after irradiation.

### 3.1. Tensile test measurements

The mechanical properties of the samples were determined, by performing tensile tests. The specimens used for these measurements had a gauge length of 15 mm with a diameter of 3 mm. The heads of the specimens had a diameter of 8 mm and the total length was 26 mm. All measurements were performed at room temperature, with a strain rate of about $2 \times 10^{-4}$/s.

Fig. 1 gives the engineering stress–strain curves, obtained for all specimens, non-irradiated and irradiated to the dose of 0.1 dpa. It is clear that all materials hardened during irradiation. However, as the shape of the curves remains the same, the initial microstructure did not change. The hardening must thus be caused by the formation of defects, which influence the motion of the dislocations.

**Table 1**
Chemical composition of the seven different alloys in wt%

| Material | Composition in wt% | | | | | | | |
|---|---|---|---|---|---|---|---|---|
| | N | C | Cu | Mn | Ni | P | Si | S |
| Pure Fe | <0.001 | <0.005 | <0.005 | 0.010 | <0.005 | <0.005 | <0.005 | <0.005 |
| Fe–C | 0.0021 | <0.005 | 0.015 | 0.015 | <0.005 | 0.007 | 0.006 | <0.005 |
| Fe + 0.1% Cu | – | <0.005 | 0.11 | 0.007 | <0.005 | <0.005 | <0.005 | <0.005 |
| Fe + 0.3% Cu | – | <0.005 | 0.315 | 0.010 | <0.005 | <0.005 | 0.012 | <0.005 |
| Fe–Mn–Ni | <0.001 | <0.005 | <0.005 | 1.09 | 0.75 | 0.005 | <0.005 | <0.005 |
| Fe–Cu–Mn–Ni | <0.001 | <0.005 | 0.105 | 1.08 | 0.72 | <0.005 | <0.005 | <0.005 |
| RPV steel | 0.07 | 0.14 | 0.064 | 1.30 | 0.75 | 0.007 | 0.195 | 0.006 |

**Table 2**
Chemical composition of the seven different alloys in wt%

| Material | Pure Fe | Fe–C | Fe + 0.1%Cu | Fe + 0.3%Cu | Fe–Mn–Ni | Fe–Cu–Mn–Ni |
|---|---|---|---|---|---|---|
| Average grain size (μm) | 250 | 350 | 125 | 177 | 88 | 88 |
| Dislocation density ($10^{13}$/m$^2$) | 7 ± 2 | 9 ± 1 | 9 ± 2 | 9 ± 1 | 3.2 ± 0.5 | 3.8 ± 0.4 |

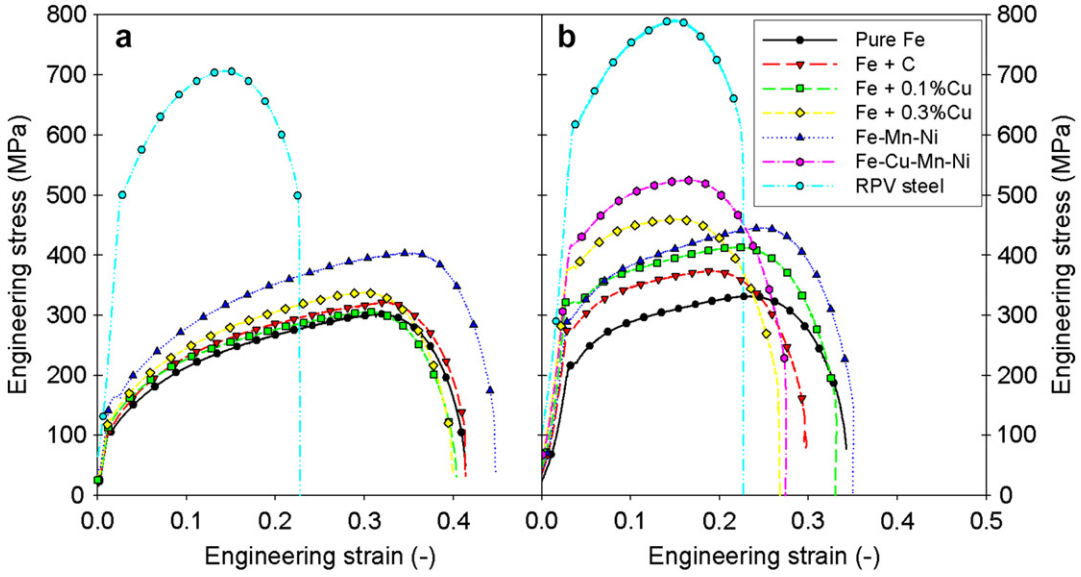


**Fig. 1.** The engineering stress–strain curves of pure iron, Fe + C, Fe + 0.1% Cu and Fe + 0.3% Cu, Fe + Mn + Ni, Fe + Cu + Mn + Ni and the RPV steel. Part (a) shows the curves for the non-irradiated specimens for all materials (except the Fe–CuMnNi alloy), while in part (b) the curves are given for the specimen, irradiated up to a dose of 0.1 dpa.

Next to hardening, embrittlement is observed, caused by the same defects. This is seen by a decrease of the total elongation.

Starting from these curves, the yield strength was calculated. Further on in this paper, the increase of yield strength in the irradiated material, compared to the non-irradiated one, will be used as reference property. In the case of the non-irradiated Fe–CuMnNi alloy, due to a shortage of material, only hardness measurements could be performed. From these data it was however possible to estimate reliably the corresponding yield strength value, based on obtained correlations.

### 3.2. Positron lifetime measurements

Non- and irradiated specimens of $10 \times 10 \times 1\ \mathrm{mm}^3$ have been first surface-polished to a mirror finish, then chemically etched using a ($HF + H_2O_2 + H_2O$)-solution to remove the deformed surface layer. The specimens, taken two-by-two in a sandwich-like fashion, with the positron source in-between, were mounted in the positron specimen holder under biologically shielded environment. The sandwich was then automatically loaded in the measurement cell between three $BaF_2$ detectors working in anti-coincidence mode. Depending on the radioactivity of the samples, the distance separating the detectors was adjusted to minimize the background. Care was taken to separate correctly the $\gamma$-peaks coming from the specimens and those related to the positrons, by following the procedure described by Jardin et al. [23]. Due to their activation, the acquisition of statistically relevant number of counts, namely at least one million, has required up to one week for each of these high-dose irradiated samples. The analysis of the obtained spectra has been performed using the LT-software [24]. The resolution of the setup was constantly checked to be about 175 ps, while the source contribution was set to 15% with a single lifetime of 393 ps. More detailed information about the experimental setup is given in [23,25]. All measurements were performed at room temperature using a $^{22}Na$ positron source, with a strength of 2 MBq, wrapped in Kapton foils.

The lifetime spectrum $N(t)$ at time $t$ obtained during the measurements is given by Eq. (1) that relates the intensities $I_i$ and the lifetimes $\tau_i$, associated with the annihilation site of type $i$. In this equation, the effect of $k$ different kinds of annihilation sites (defects) is superposed.

$$N(t) = \sum_{i=1}^{k+1} \frac{I_i}{\tau_i} \exp\left(-\frac{t}{\tau_i}\right) \tag{1}$$

The positron lifetime $\tau$ carries information about the electron density at the annihilation site. The annihilation rate $\lambda$, the reciprocal of the lifetime, is given by the overlap of the positron density $n_+(\mathbf{r})$ and the electron density $n_-(\mathbf{r})$, according to the following Eq. [26]:

$$\lambda = \frac{1}{\tau} = \pi r_0^2 c \int n_-(\mathbf{r}) \gamma(\mathbf{n}_-(\mathbf{r})) \mathbf{n}_+(\mathbf{r}) \mathbf{dr} \tag{2}$$

Here $r_0$ is the electron radius, $c$ is the speed of light and $\gamma(n(\mathbf{r}))$ is the enhancement factor. Theoretical investigations on these values have been carried on by Kuriplach et al. [27] and others [28]. The electron density is related to, amongst other things, the amount of vacancies near the annihilation site.

To correlate the lifetime- and the intensity-parameters with the real properties of the defects, we need to solve the following set of differential equations:

$$\frac{dn_B}{dt} = -\left(\lambda_B + \sum_{i=1}^{k} \kappa_i\right) n_B + \sum_{i=1}^{k} \delta_i n_{Di} \tag{3}$$

$$\frac{dn_{Di}}{dt} = \kappa_i n_B - (\lambda_{Di} + \delta_i) n_{Di} \tag{4}$$

In these equations $B$ and $D_i$ denote the free (bulk) and the trapped (defect) state, respectively, while $\kappa$ is the trapping rate and $\delta$ is the detrapping rate. When these equations are solved with the knowledge of all parameters, it is possible to determine the number of each type of defects using the intensities $I_i$.

### 3.3. Coincidence Doppler broadening measurements

The specimens for CDB have been prepared in the same way as the ones for PLT. The CDB measurements have been performed as already described by Verheyen et al. [22]. The analysis of the results have been made using CDB ratio curves, obtained by normalizing the momentum distribution to the one of unirradiated defect-free pure Fe. The S- and W-parameters were extracted from each spectrum. They are defined respectively as the ratio of low-momentum ($|cp_L| < 2.5 \times 10^{-3}$ mc) and high-momentum ($15 \times 10^{-3}$ mc $< |cp_L| < 25 \times 10^{-3}$ mc) regions in the CDB spectrum

to the total region ($c$ is the speed of light and $p_L$ is the longitudinal component of the positron–electron momentum along the direction of the $\gamma$-ray emission).

Since the total curves are normalized, the $S$- and $W$-parameters will be necessarily correlated. Nevertheless, both parameters will carry different information. The valence electrons can only give rise to a small difference in the energy of the annihilation $\gamma$-rays, while the core electrons can lead to much larger energy changes. The former will thus contribute to the peak of the CDB curves, and will therefore be observed by the $S$-parameter, which therefore carries mainly information about the open-space defects (e.g. vacancies). The latter, on the other hand, will contribute to the whole background of the spectrum. Therefore, the $W$-parameter qualifies these electrons. Moreover, the changes in the $\gamma$-energies due to the core electrons will possess specific information about the corresponding chemical species.

## 4. Results and discussion

### 4.1. Tensile test results

In Fig. 2, the obtained yield strength increase after irradiation is shown for each alloy. The average error bar to be associated with the data, given in the figure, is ±6% of the yield strength value. This error thus varies in-between ±5 MPa for the non-irradiated pure iron and ±35 MPa for the steel irradiated to the highest dose. Next to these results, some values of steels are added, which are found in literature [29]. It can be seen that the irradiation-induced hardening depends strongly on the material composition. The trend for high-Cu steels (full symbols), for example, which is saturating after a certain dose, is obviously different from the trend of low-Cu steels (empty symbols). These latter steels seem to be linearly dependent on the irradiation dose. The region indicated in the figure corresponds to 30% error starting from the trend line for the high-Cu steels given by the results from literature.

In pure iron, the irradiation-induced hardening at low dose is rather high, almost 100 MPa. But only a small increase is observed during further irradiation up to 0.1 dpa. A saturation-like behaviour is thus observed for this alloy. This saturation is much less pronounced, when carbon is added to the alloy. At low dose, the hardening of both alloys is comparable, while at the highest dose, an increase of about 50 MPa is found in the Fe–C alloy. As it will be briefly discussed later on, it may be speculated that this is the consequence of the presence of a higher density of self-interstitial atom (SIA) clusters, due to a larger number of nucleation sites at the carbon atoms. These clusters act as obstacles to the dislocation motion.

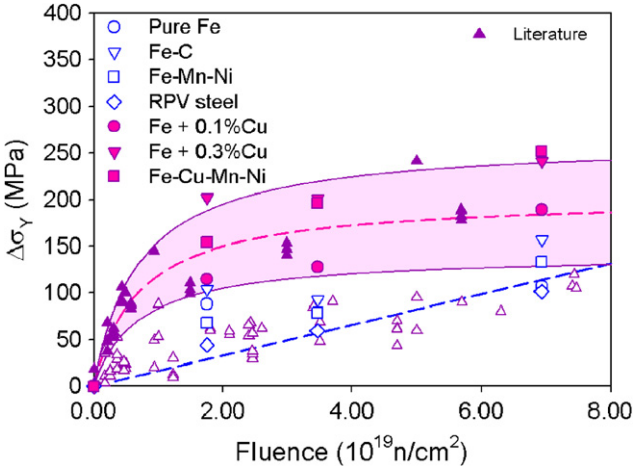


**Fig. 2.** The hardening (change of yield strength of the irradiated measurement compared to the unirradiated measurement) for all materials is illustrated in function of the neutron fluence. Some results found in literature are added. The empty symbols symbolize the low-Cu steels, while the full symbols are results of high-Cu steels. For both type of steels a trend line is given, and for the high-Cu steels a region with an error of 30% is added.

The binary Fe–Cu alloys follow the trend indicated by the high-Cu steels. When 0.1% of copper is present in the alloy, the hardening is at the lower limit of the region shown in the figure, while the alloy containing 0.3% of copper is at the upper limit. The alloys exhibit a clear trend of substantially enhanced hardening with increasing copper concentration. The enormous increase of hardness after irradiation is certainly due to the formation of copper precipitates, as will be discussed later on. It has been previously demonstrated that most of the precipitation occurs already at the start of irradiation for the alloys discussed in this paper (see [22,30]). This can also be seen in Fig. 2. At the highest irradiation dose presently studied, the formation of precipitates will thus already be complete, and the hardening will be saturated.

Fig. 2 also shows that when manganese and nickel are added to the model alloys, the behaviour is quite different. The Fe–MnNi alloy follows the trend of the low-Cu steels, although it should be mentioned that the results for this alloy are a little higher than the trend line. This is most probably caused by a different initial microstructure in the model alloy compared to those of the used steels. But for the alloy which contains also copper next to the manganese and nickel, the hardening increases drastically. Nevertheless, the hardening does not saturate as it was indicated by the high-Cu steels. It may be seen that after an initial hardening, caused by the copper-rich precipitates, the irradiation-induced hardening of this alloy follows a trend parallel to the one of the one of low-Cu steels. We thus believe that the hardening mechanism associated with the presence of copper is independent of the one associated with the presence of manganese and nickel.

As the increase of irradiation hardening due to the copper-addition is higher, the effect of this element is the predominant one in medium- and high-copper steels [31]. Therefore, the effect of copper has been specifically investigated for many years (e.g. [8,32,33]). It is thus by now well-known that, already at very low dose, some copper-rich precipitates are formed [8,33]. These precipitates hinder the dislocation motion, thereby causing hardening [34]. Once the precipitates are formed, however, the Cu-rich precipitate contribution to the irradiation-induced hardening saturates relatively quickly [2,3,30,31]. A higher copper concentration in the alloy leads to the formation of more precipitates, and thus to a higher hardening component, but the trend to saturation with dose remains unchanged.

In contrast to higher-copper steels, the effect of manganese and nickel is not negligible in low-copper steels. This effect may even become dominant for high enough doses [31,35]. For this reason, research should now be focused on this hardening effect as well. Accordingly, this paper tries to give some hints about the mechanisms underlying this hardening effect, using the PAS results.

The hardening behaviour of the low-copper RPV steel, examined in this work, follows exactly the trend indicated by the results from literature. In addition, it is important to note that this behaviour is very close to the one of the alloy containing manganese and nickel and no copper. The small difference can probably be explained by the richer chemical composition of the steel and/or the different initial microstructure (the model alloys are purely ferritic, while the steel is ferritic/bainitic).

### 4.2. Positron annihilation spectroscopy results

#### 4.2.1. Influence of defects on the PAS results

It has been mentioned before, that the positron affinity to the defects is related to the electron density surrounding them.

Positrons are thus very sensitive to vacancy-type defects, but they are much less sensitive to self-interstitial clusters and loops. On the other hand, alloying elements have different electron densities, compared to the iron matrix [36]. It is reported that the affinity of positrons to iron is −3.84 eV. It is thus known that, for example, copper and nickel have a higher positron affinity than iron (−4.81 eV and −4.46 eV, respectively), while carbon and manganese have a lower affinity (−2.50 eV and −3.72 eV, respectively). Therefore, defects containing copper and/or nickel trap the positrons more easily, while the opposite occurs for defects containing carbon and manganese.

As mentioned, the low momentum part of the CDB results, or *S*-parameter, is especially due to positrons annihilating with valence electrons of atoms near the annihilation site. Therefore, this part of the curve contains more information about the vacancy behaviour in the material. The high momentum part, or *W*-parameter, on the other hand, deals with the core electrons of the atoms. This parameter is thus a fingerprint of the chemical species near the annihilation sites. The CDB spectra for all elements used in this paper can be found in the literature, e.g. [37,38]. It is for instance known that copper and nickel have a similar behaviour. They both have an elevated *W*-parameter, although this effect is higher for copper than it is for nickel. PAS is thus an excellent technique to identify defects containing one or the other of these two elements. Nevertheless, it is difficult, if not impossible, to distinguish between them, when they are simultaneously present.

The lifetime results can provide information on the number density of vacancy clusters (intensity) and the average amount of vacancies per cluster (lifetime component), if the trapping and detrapping rates are rigorously obtained. Pure defect-free iron has only one lifetime component, equal to 107 ps. When defects appear, more lifetime components can be deconvoluted. Generally, the spectrum is resolved into two components. The first one is assigned to the annihilation with the iron–matrix, while the second one reflects the presence of other annihilation sites, such as irradiation-induced defects. For vacancy-type defects, the latter component increases with the number of single vacancies that form a cluster, up to a size at which the cluster can be defined as a void [27]. The intensity of the second component depends on the amount of defects contributing to the process of annihilation.

The lifetimes for pure defect-free copper and nickel, found to be 122 ps and 110 ps, respectively, are very close to the one for pure defect-free iron. Vacancy-free copper and nickel precipitates will thus contribute to the first component (or the bulk component) rather than to the second component. Therefore, only the precipitates and solute atoms associated with vacancies can be seen within the second PLT component.

*4.2.2. Results*

Fig. 3 gives the results of CDB for all alloys, irradiated to 0.1 dpa. The numbers shown, correspond to the ratio of the values obtained from the measurement of the investigated alloys to the one of non-irradiated pure iron. The *increase* is given as the difference between the irradiated value and the non-irradiated one. The values for the non-irradiated materials are all about 1, as these materials do not contain any defects or positron affinitive places before irradiation. The error bar to be associated with the reported values is ±0.000874 for *S* and ±0.00185 for *W*.

During irradiation more vacancies are formed, thus the *S*-parameter increases. At the same time fewer positrons are able to annihilate with inner-shell electrons (as they annihilate with outer-shell electrons at vacancies), and the *W*-parameter decreases. The irradiated pure iron, in Fig. 3, has thus a positive *S*-parameter variation and a negative *W*-parameter variation. If some carbon is added, a decrease of *S* is observed, while *W* remains almost the same. The defects where the positrons annihilate thus have the same chemical environment in both cases, but the presence of carbon seems to reduce the number of vacancies in the observed vacancy-type defect clusters.

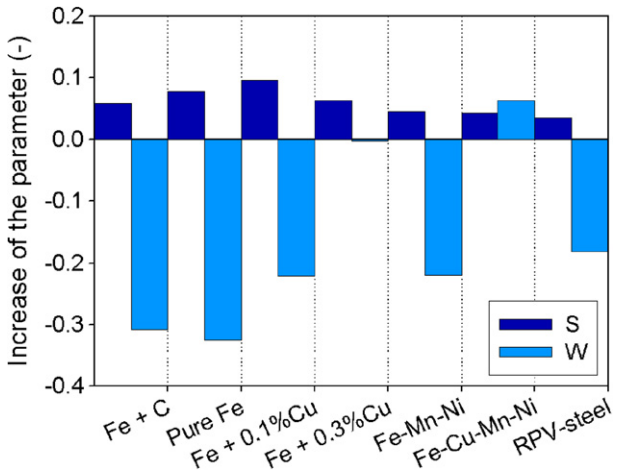


**Fig. 3.** The low (*S*-parameter) and high (*W*-parameter) momentum part of the CDB results are shown for all materials. The *increase* of the parameter is given as the difference between the value for the irradiated specimen and the one for the non-irradiated specimen.

The binary iron–copper alloys show on the one side an increase of *W* with increasing Cu content (less negative variation compared to the pure iron). This indicates the presence of Cu-rich precipitates. The alloy with more copper contains more precipitates and has thus a higher *W*-value. On the other side, the behaviour of *S* is more complicated to rationalize. For the medium-copper alloy an increase of the *S*-value compared to iron is observed. In the higher-copper alloy, however, the *S*-parameter decreases. This apparently contradicting result will be discussed and explained later on.

When manganese and nickel are added to pure iron, *W* experiences a modest increase (less negative than iron), ascribable to the presence of nickel, while *S* decreases drastically (see Fig. 3). The latter effect can be interpreted as a sign that the vacancy clusters remain very small, much smaller than in pure iron. The addition of copper to the Fe–MnNi alloy leads, as expected, to an enormous increase of the *W*-value. This huge increase in *W* contributes to a further decrease of *S*, as a result of the equilibrium between the two parameters.

Similar considerations can be made for the RPV steel. This steel contains the same amount of nickel as the model alloy, but it has a very low concentration of copper. As a result of this, the effect of nickel is the most explicit. The *S*-parameter is somewhat smaller than expected. This must be interpreted in terms of fewer or smaller vacancy clusters, caused by the presence of other chemical species.

Fig. 4 shows the PLT results for all the materials investigated. The average error bar to be associated with the reported values is about ± 0.009 for the intensity (Fig. 4(a)) and ±3.5 ps for the lifetime (Fig. 4(b)). Here, it is seen clearly that there are only a few (low intensity) vacancy clusters created in pure iron, after irradiation to 0.1 dpa, but these clusters are found to be relatively big (the lifetime suggests somewhat less than 10 vacancies per cluster in average). For the Fe–C alloy the same observations can be made. Nevertheless, the positron signal intensity is a little lower, which indicates that more positrons annihilate in the bulk material. This is consistent with the observations from CDB.

The presence of copper increases the intensity of the second component (Fig. 4(a)) in the binary Fe–Cu alloys, i.e. the number of detected vacancy clusters rises. The amount of vacancies per

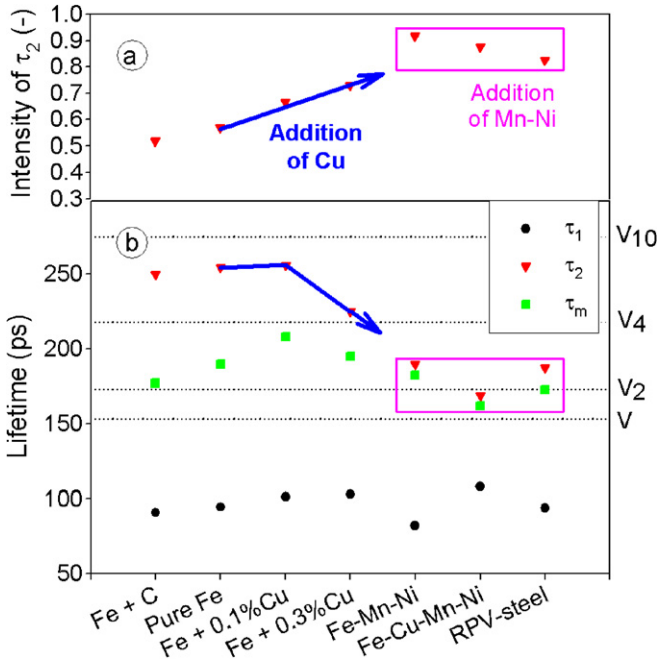


**Fig. 4.** The positron lifetime results for all materials can be seen. The results are divided into two lifetime components ($\tau_1$ and $\tau_2$) and their average is given as well ($\tau_m$). This is given in part (b) of the figure. $I_2$ (a) is the intensity of $\tau_2$ ($I_1(\tau_1) + I_2(\tau_2) = 1$). In the figure, the theoretical values of positron lifetime in V-clusters obtained by Kuriplach et al. [27] are also reported. The effect of a copper and a manganese–nickel addition is visible.

cluster stays approximately the same as in pure iron when 0.1% of copper is added, while this amount decreases in the alloy with 0.3% of copper, where more precipitates are present (Fig. 4(b)).

For the alloys containing manganese and nickel the intensity of the second component spectacularly increases to more than 90% (Fig. 4(a)). This means that almost all positrons annihilate near defects and almost none annihilate in the bulk-material. The vacancy clusters observed are, however, very small (Fig. 4(b)). This supports the results of CDB. The addition of copper causes a less pronounced intensity increase, while the clusters contain even less vacancies.

The result of the low-Cu steel resembles closely the results of the Fe–MnNi alloy. The second component of the steel is almost the same as the one of the Fe–MnNi alloy, while its intensity is a little lower.

### 4.3. Binding energies of the investigated elements with vacancies and interstitials

For the understanding of the above results, it is necessary to take into account what is known concerning the binding energies of the investigated atomic species with vacancies and self-interstitials, as well as with each other. These energies will play a significant role in the microstructural evolution, produced under irradiation, that results in the changes observed in the PAS and tensile test results. For the solute-solutes and vacancy-solutes interaction, the outcome of [39] has been used. Vincent et al. [40] gives the self-interstitial interaction with solute atoms in α-Fe. And, the interaction of an interstitial carbon atom with intrinsic point defects in α-Fe has been studied in [41]. All calculations have been performed using the Vienna ab initio simulation package (VASP) and are therefore consistently comparable.

For the atom description scheme, the ultrasoft pseudopotential (USPP) approximation has been used, in the published calculations. However, more recently the projector augmented wave (PAW) approximation has been compared to the USPP method, and the results obtained with the PAW method are found to be more reliable. Some preliminary PAW results are provided by Olsson [42] (negative values indicate repulsion, positive attraction). For the vacancy-solute binding energy for nickel, the values 0.12 and 0.20 eV were found, respectively, in first (1 nn) and second (2 nn) nearest neighbours. The outcome for manganese is 0.21 eV in 1 nn and 0.14 eV in 2 nn. The binding energy between a mixed-dumbbell and a solute atom is 80.16 eV for nickel and 0.57 eV for manganese.

From Table 3 of [39] it can be seen that all elements investigated in this paper tend to be bound to vacancies in both first and second nearest neighbour position. Thus all these elements are likely to be dragged by a vacancy. This remains true for nickel and manganese according to the PAW results, given before. As the binding energy between two solute atoms, aside from copper, is negative (see Table 2 of [39]), only copper-rich precipitates will be easily formed. In addition, atomistic studies show that vacancy clusters are preferentially associated to Cu atoms [43]. This is in agreement with the interpretation of previous PAS experiments [8], as well as ours, as it will be discussed later on in this paper.

The interaction of the elements with SIAs is different (Table 3 of [40]). Nickel will not be bound to an SIA in any case, while copper will be bound very weakly, as first nearest neighbour, but only in one specific configuration. Once the copper and the SIA are bound, they will tend to dissociate immediately, as it is shown in [40]. Manganese, on the other hand, has a very strong binding energy with the SIA. This value is even higher, when the PAW method is used. Moreover, in presence of manganese, Fe–Mn mixed-dumbbells are likely to be formed and they are able to migrate in all three dimensions [40], providing a means to transport Mn atoms to sinks for SIAs (for example to SIA clusters).

Finally, the interstitial carbon atom binds vacancies very strongly (Table IX of [41]), while single SIAs seem not to be bound at all (Table XIII of [41]). However, a more recent investigation [44] suggests that the dumbbell is weakly attracted by a carbon atom (binding energy up to about 0.19 eV), when located at a mutual distance of more than one lattice parameter. Furthermore, recent atomistic simulations suggest that a single C atom may trap an SIA cluster with a binding energy between 0.5 eV and 1 eV [45].

### 4.4. Discussion

Under neutron irradiation, damage is produced by displacement cascades. Not only single vacancies and SIAs are produced in a displacement cascade, but also some small vacancy and a few sizeable SIA clusters [5,6]. In pure iron, these small defects are free to move according to their diffusion properties, until they annihilate or accumulate in bigger loops and voids. All these defects can cause irradiation hardening, because dislocations can be pinned by them. However, PAS is only sensitive to the vacancy clusters and their chemical environment. *S* increases, *W* decreases, whereas a second component appears in the PLT spectrum.

The Fe–C alloy, studied in this work, contains a non-negligible amount of carbon impurities, with which both vacancy- and self-interstitial-type defects will interact. The PAS results indicate only slight differences from pure iron. The similar *W*-parameter suggests that the chemical environment at the annihilation sites is the same in Fe and Fe–C. However, if C was associated with vacancies, the technique would not be sensitive to it, due to its low affinity to positrons. The minor increase of *W* may be due to the presence of a small quantity of copper (see Table 1) or simply to the slight decrease of the *S*-value. The decrease of *S* (Fig. 3), as well as the lower intensity in the second PLT component (Fig. 4) may be caused by a somewhat enhanced recombination of vacancies with SIAs and a hindered growth of vacancy clusters. Indeed, as vacancies are relatively strongly trapped by carbon atoms, their effective diffusivity will be reduced (a well-known effect of C on vacancies,

see e.g. [46]). So, they will have more opportunities to annihilate with single SIAs, before forming clusters. This could be the reason, why fewer vacancies are observed in this alloy, in comparison to pure iron. However, since the vacancy cluster population in Fe–C and in pure Fe is essentially the same (the differences are very small), the irradiation hardening increase in this material is most probably caused by a difference in the population of SIA clusters. A higher density of SIA clusters will correspond to an increased number of pinning points for the dislocations and thus more hardening will appear. This can be explained by the suggestion of an attraction between the carbon atom and a single dumbbell pair, as it was illustrated earlier. The C atoms will provide some additional nucleation sites for SIA clusters that, being trapped, cannot disappear at sinks, thereby increasing their density compared to pure Fe. In addition, due to the trapping effect of C, growth of loops by coalescence of SIA clusters will be hindered, thereby keeping their density higher.

The addition of copper to iron hardens the material drastically. Based not only on our results, but also on the abundant literature on the matter, we know that this hardening is due to the appearance of Cu-rich precipitates. Nagai et al. [8] have suggested that copper atoms are dragged by migrating vacancies to form copper–vacancy complexes. Recently, this dragging of copper was also shown by atomistic simulations [47,48]. This is a consequence of the relatively high binding energy between a copper atom and a single vacancy, up to the second nearest neighbour distance. This not only provides a mechanism for the two species to migrate together, but is also the driving force for the easy nucleation and growth of the copper–vacancy complexes. These will further evolve into Cu precipitates with a number of associated vacancies. Our results confirm this point of view. As a large fraction of the positrons annihilate at these vacancy-rich precipitates, and therefore near copper atoms, the *W*-value increases significantly as compared to pure iron. At the same time, positrons interact with the vacancies in these precipitates and therefore also the *S*-value and the intensity of the second PLT component increase. The very high second PLT component itself implies a high vacancy-to-copper ratio in the defects.

If more copper is present, as it is in the Fe + 0.3% Cu alloy, even more vacancies become visible to PAS, due to the attraction of positrons towards copper–vacancy complexes. This is seen in the increase of the intensity of the second PLT component. But in parallel the *S*-parameter is found to decrease. This is easily explained considering that, the same amount of vacancies are created during irradiation at the same dose in both Fe-Cu alloys (the presence of small quantities of Cu is known not to influence the number of produced Frenkel pairs [49]), while more copper atoms are available in the matrix. So, more precipitates will be formed and the vacancies will be distributed among them. Therefore, in each of them, the vacancy-to-copper ratio will be lower. And thus, proportionally more core electrons are used for positron annihilation, and less valence electrons. This is the origin of the *S*-decrease, accompanied by an important increase of *W*, while the decrease of the second PLT component is due to the lowering of the vacancy-to-copper ratio, i.e. the lowering of the average number of vacancies in the clusters associated to the copper precipitates.

For the alloys containing manganese and nickel a second irradiation-hardening mechanism is proposed, which is independent of the mechanism caused by copper. However, as it is mentioned before, manganese has almost no effect on the PAS results; the positrons will rather be trapped by defects containing nickel or copper. Information on this second hardening mechanism can therefore only be obtained in an indirect way and here is where the hints coming from computer-modelling become useful. All three elements (Cu, Mn and Ni) have a binding energy with vacancies of the same order of magnitude. Therefore, migrating vacancies will all end up being bound to atoms of all three elements. It has been mentioned before that the binding energy between two solute atoms, different from copper, is negative, so only copper clusters will be easily formed (if Cu is present), and some vacancies will be bound to them. The remaining vacancies (again produced in the same amount as in the other materials) will be dispersed in the matrix, bound to unclustered solute atoms, thereby being hindered from forming clusters of appreciable size. We believe that this is the reason why, in both the Fe–MnNi and the Fe–CuMnNi alloy, an immense decrease in the *S*-parameter and second PLT component is observed, compared to the alloys containing no manganese and nickel. As this implicates that there are a large amount of very small vacancy-type defects, almost uniformly distributed in the matrix, where the positron can be trapped, the intensity of the second PLT component augments above 90%. Thus, almost no positrons annihilate in the matrix. The fact that the alloy with no copper has a *W*-value comparable with that of the Fe + 0.1% Cu alloy can be understood in a satisfactory way. Although the *W* increase due to nickel is lower than that due to copper, the nickel concentration is higher, which leads to these comparable values.

The additional presence of copper in the Fe–CuMnNi alloy causes the vacancies to be dispersed even more. Di-vacancy clusters are reduced only to single vacancies. Therefore the *S*-parameter and the second component decrease even more. But, again more positrons annihilate with the core electrons of copper and nickel, leading to a huge increase of the *W*-parameter, which is even higher than the one caused by the highest copper concentration in the binary Fe–Cu alloys. The small decrease in the intensity of the second PLT component can be explained by noticing that the first PLT component increases in this alloy. Therefore, it can be assumed that some positrons annihilate near copper or nickel atoms free from vacancies, as these defects will have a positron lifetime comparable to the one of the bulk material. This would be an additional explanation for the extreme increase of the *W*-value. At the same time, the dispersion of vacancies in the matrix, bound by manganese and nickel atoms, reduces the number of vacancies bound to the copper atoms, thereby retarding the irradiation-induced precipitation of copper via vacancy dragging. Nonetheless, as it will be discussed in future work, there is clear evidence that the precipitation of copper is already completed at 0.1 dpa.

This interpretation of the PAS data is also largely valid for the RPV steel. This steel contains the same amount of nickel as the model alloy and a very low concentration of copper. As a result, the specific effect of nickel is here more explicit. Small fluctuations, as compared to the model alloys, may be due to the more complex chemical composition. It should be mentioned as well that for the result of both the tensile tests and the PAS measurements, the low-Cu steel resembles most the Fe–MnNi alloy. This emphasizes that manganese and nickel must play an important role in the hardening and embrittlement of these steels.

Clearly, the above explanations, based on the presence of uniformly distributed mono- and di-vacancy defects cannot explain the additional irradiation hardening seen in the tensile tests for the alloys containing manganese and nickel. The dislocations will move through these defects without major problems. So, the existence of an additional hardening feature should be invoked, which must be different from the copper precipitate hardening and also not related to the vacancy-type defects. As it was stated before, manganese is strongly bound to self-interstitials. Therefore, it can be speculated that manganese decorates the SIA loops and, by lowering their energy, it reduces drastically the mobility of the loops. Similar to what has been postulated to happen in Fe–C, but in a more pronounced way, this will lead to the formation of a larger density of smaller loops, as compared to alloys free from Mn. Nickel may also end up decorating these small, virtually immobile loops, dragged by vacancies that annihilate with some of the SIAs

present. This phenomenon is invisible to PAS, but it would be able to cause the additional hardening.

Another possibility could also be that vacancy-manganese and/or vacancy–nickel pairs, in spite of the mutual repulsion between single Mn and Ni atoms, succeed in transporting these solutes, until they agglomerate (in the same way as it has been seen for the vacancy-copper combination) eventually forming Mn and Ni precipitates, supposing that a Mn- and Ni-rich phase can be stable, or meta-stable, in bcc Fe. These precipitates should not contain large amounts of vacancies, as PAS does not reveal the existence of vacancy clusters associated to them. Due to the low intermetallic binding energy, the nucleation of these features will occur at a much lower rate than Cu precipitation and therefore they would only become visible after higher irradiation doses. In the literature, this phenomenon has been referred to as the formation of 'late blooming phase' [35]. Further investigations need to be performed, using other experimental techniques, such as TAP, to identify and study these Mn- and Ni-rich defects and post-irradiation annealing experiments may help to discriminate between the two above suggestions.

Whichever its nature and origin, it has been observed that this second hardening component, caused by the presence of manganese, becomes predominant at higher doses [3]. Nevertheless, the dose examined here is not yet sufficient to observe a considerable influence of this component. At the current dose, most of the hardening is still due to copper precipitation. This can be observed in Fig. 5, where the alloys are separated into Cu-rich and Cu-free alloys in the $W$–$S$–$\Delta\sigma$ space. The former group reveal a high irradiation-induced hardening, while this hardening is relatively low for the latter one. The alloys containing copper, characterized by their high $W$-value, all show a marked hardening. Due to the presence of a large amount of vacancies in the copper-rich cluster of the Fe + 0.1% Cu alloy (indicated by a high $S$-value), W decreases remarkably. Nevertheless, the hardening due to copper-precipitates is still important.

On the other hand, it is clear that the size of the vacancy clusters has a much less pronounced influence on the yield strength increase. Indeed, both groups of materials (with and without copper) are scattered over the whole $S$-range. In fact, in the Cu-rich materials the vacancy cluster effect on hardening, if any, is totally hidden by the Cu precipitates, as they are always associated with these precipitates. So, the hardening features should be better defined as copper–vacancy complexes. In Cu-free materials no correlation can be found between $S$ and the hardening. Therefore, it seems to be likely that not the vacancy-type of defects determines the irradiation-induced matrix damage hardening, but, instead, the interstitial-type defects play the major part in it. These speculations need of course to be, and can be, confirmed by looking at the results of other microstructural characterization techniques applied to the same materials. However, the PAS evidence, combined with a few computer-modelling results, is already sufficient to make this scenario highly plausible.

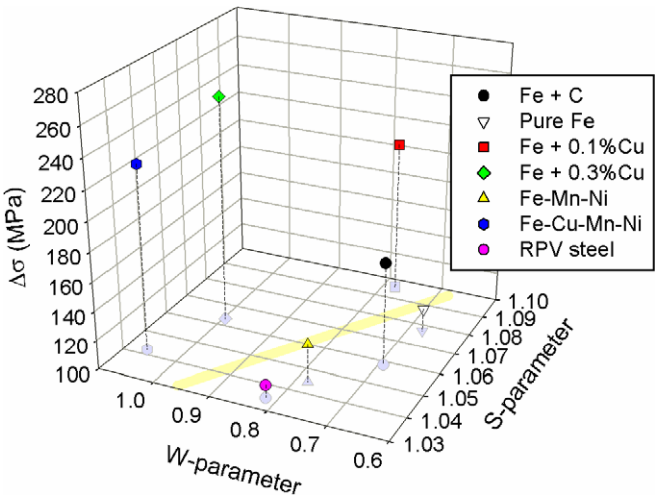


**Fig. 5.** The hardening results for all materials, shown in Fig. 2 are plotted in function of the $S$- and $W$-parameter. Two different groups are visible. The first one contains the Cu-rich alloys, while the second one consists of the alloys without copper.

## 5. Conclusions

Positron annihilation spectroscopy, both positron lifetime and coincidence Doppler broadening, are powerful techniques to analyze Cu-rich precipitates and all kinds of defects containing vacancies. SCK•CEN has the facilities which allow analyzing active specimens with high accuracy. The positron lifetime results depend on the size and the volume fraction of vacancy clusters, and therefore PLT can extract information on the mean size of the defects. On the other hand, CDB can give information on the chemical environment of the annihilation sites, due to the high affinity of positrons to some alloying elements. By means of the combination of these two techniques, the growth of precipitates, the formation (or not) of vacancy clusters and their association (or not) with clustered and unclustered alloying elements can be traced.

The experiments conducted for this paper were used to interpret the corresponding hardening results. As expected, copper precipitation was already observed at an early stage of irradiation, and it was found to be the main cause of hardening in the alloys containing this element. However, this contribution to the hardening is known to saturate at higher doses. Any further increase of the hardening can be only explained in terms of the effect of the so-called matrix damage. The nature of this matrix damage, generally described as 'voids and interstitial loops', but in fact so far elusive, is here seen to be strongly affected by the presence of Mn and Ni. Different from the alloys containing no Mn and Ni, the matrix damage contribution to hardening keeps on growing with dose. Since ab initio calculations show that the Mn is preferably located in interstitial positions, it is suggested that this contribution comes from SIA loops decorated and trapped by Mn atoms. These Mn-decorated loops are also likely to be decorated by Ni, dragged by vacancies that recombine with the SIAs in the loops. An alternative explanation is that Mn and Ni precipitates, whose nucleation is much slower than that of Cu precipitates, are formed. These stable or meta-stable phases should not contain large quantities of vacancies.

The hardening in low-Cu steels is thus different from the one in high-Cu steels. It was observed that most of the irradiation-induced hardening in RPV steels and their model alloys irradiated up to a dose of 0.1 dpa was still due to copper precipitation. But even at this irradiation dose, matrix damage already played an important role. As copper precipitation was fully completed by this dose, the influence of matrix damage is expected to become more manifest when the material is irradiated up to a higher dose. Therefore, discriminating between the two possibilities of matrix damage requires further studies, including a detailed analysis of specimens irradiated up to a dose of 0.2 dpa and post-irradiation annealing experiment, which will be the subject of future work.

## Acknowledgements

This work was partly financed by the European Union in the framework of the PERFECT project, under contract FI60-CT-2003-5088-40.

## References


[1] S.B. Fisher, J.E. Harbottle, N. Aldridge, Phil. Trans. R. Soc. Lond. A 315 (1985) 301.
[2] C.A. English, J.M. Hyde, S.R. Ortner, in: Proceedings of International Symposium on the Mechanisms of Materials Degradation and Non-Destructive Evaluation in Light Water Reactors, Osaka (Japan) (2002) 53.
[3] L. Malerba, E. van Walle, C. Domain, S. Jumel, J.C. Van Duysen, in: Proceedings of the 10th International Conference on Nuclear Engineering, ICONE-10, The American Society of Mechanical Engineers (2002).
[4] W.J. Phythian, C.A. English, J. Nucl. Mater. 205 (1993) 162.
[5] L. Malerba, J. Nucl. Mater. 351 (2006) 28.
[6] D. Terentyev, C. Lagerstedt, P. Olsson, K. Nordlund, J. Wallenius, C.S. Becquart, L. Malerba, J. Nucl. Mater. 351 (2006) 65.
[7] Y. Nagai, M. Hasegawa, Z. Tang, A. Hempel, K. Yubuta, T. Shimamura, Y. Kawazou, A. Kawai, F. Kano, Phys. Rev. B 61 (2000) 6574.
[8] Y. Nagai, Z. Tang, M. Hasegawa, T. Kanai, M. Saneyasu, Phys. Rev. B 63 (2001) 134110.
[9] P. Asoka-Kumar, B.D. Wirth, P.A. Sterne, R.H. Howell, G.R. Odette, Philos. Mag. Lett. 82 (2002) 609.
[10] K. Fujii, K. Fukuya, N. Nakata, K. Hono, Y. Nagai, M. Hasegawa, J. Nucl. Mater. 340 (2005) 247.
[11] M. Eldrup, B.N. Singh, J. Nucl. Mater. 251 (1997) 132.
[12] M.J. Puska, R.M. Nieminen, Rev. Mod. Phys. 66 (1994) 841.
[13] W. Salgueiro, A. Somoza, O. Cabrera, G. Consolati, Cement Concrete Res. 34 (2004) 91.
[14] Y.C. Jean, Microchem. J. 42 (1990) 91;
Y.C. Jean, Mater. Sci. Forum 175–178 (1995) 59.
[15] Y.C. Jean, P.E. Mallon, D.M. Schrader, Principles and Applications of Positron and Positronium Chemistry, World-Scientific, London, 2003.
[16] R. Krause-Rehberg, H.S. Leipner, Positron Annihilation in Semi-conductors, Springer, Berlin, 1999.
[17] J.T. Buswell, J.P. Highton, CEGB, Berkeley Nuclear Laboratories, TPRD/B/0787/R86, 1986.
[18] G.H. Dai, P. Moser, J.C. Van Duysen, in: Proceedings of the IXth International Conference on Positron Annihilation, Szombathely (Hungary) (1991) 941.
[19] R.G. Carter, T. Onchi, N. Soneda, K. Dohi, J.M. Hyde, C.A. English, M.T. Hutchings, W. Server, J.F. Coste, J.C. Van Duysen, in: Proceedings of the IVth International Symposium on the Contribution of Materials Investigation to the Resolution of Problems Encountered in Pressurized Water Reactors, Fontevraud (France) (1998) 89.
[20] M. Valo, R. Krause, K. Saarinen, P. Hautojarvi, J.R. Hawthorne, in: R.E. Stoiler, A.S. Kumar, D.S. Gelles (Eds.), Effects of Radiation on Materials: 15th International Symposium, ASTM 1125, ASTM, Philadelphia (USA) (1992) 172.
[21] M. Eldrup, B.N. Singh, J. Nucl. Mater. 323 (2003) 346.
[22] K. Verheyen, M. Jardin, A. Almazouzi, J. Nucl. Mater. 351 (2006) 209.
[23] M. Jardin, M. Lambrecht, A.A. Rempel, Y. Nagai, E. van Walle, A. Almazouzi, Nucl. Instr. and Meth. A 568 (2006) 716.
[24] J. Kansy, Nucl. Instr. and Meth. A 374 (1996) 235.
[25] M. Jardin, A. Almazouzi, M. Lambrecht, A.A. Rempel, Y. Nagai, E. van Walle, Phys. Status Solidi C 4 (2007) 4001.
[26] R.M. Nieminen, M.J. Manninen, in: P. Hautojärvi (Ed.), Positrons in Solids, Springer-Verlag, Berlin, 1979, p. 145.
[27] J. Kuriplach, O. Melikhova, C. Domain, C.S. Becquart, D. Kulikov, L. Malerba, M. Hou, A. Almazouzi, C.A. Duque, A.L. Morales, Appl. Surf. Sci. 252 (2006) 3303.
[28] P.A. Sterne, J.E. Pask, B.M. Klein, Appl. Surf. Sci. 149 (1999) 238.
[29] R. Chaouadi, R. Gérard, J. Nucl. Mater. 345 (2005) 65.
[30] M. Lambrecht, M. Jardin, A. Almazouzi, Phys. Status Solidi C 4 (2007) 3477.
[31] J.T. Buswell, W.J. Phythian, R.J. McElroy, S. Dumbill, P.H.N. Ray, J. Mace, R.N. Sinclair, J. Nucl. Mater. 225 (1995) 196.
[32] M. Perez, F. Perrard, V. Massardier, X. Kleber, A. Deschamps, H. De Monestrol, P. Pareige, G. Covarel, Philos. Mag. 85 (2005) 2197.
[33] P.J. Pareige, K.F. Russel, M.K. Miller, Appl. Surf. Sci. 94/95 (1996) 362.
[34] K.C. Russell, L.M. Brown, Acta Metal. 20 (1972) 969.
[35] G.R. Odette, G.E. Lucas, Radiat. Eff. Defects Solids 144 (1998) 189.
[36] M.J. Puska, P. Lanki, R.M. Nieminen, J. Phys. Condens. Matter. 1 (1989) 6081.
[37] P. Asoka-Kumar, M. Alatalo, V.J. Ghosh, A.C. Kruseman, B. Nielsen, K.G. Lynn, Phys. Rev. Lett. 77 (1996) 2097.
[38] Y. Nagai, Z. Tang, M. Hasegawa, Rad. Phys. Chem. 58 (2000) 737.
[39] E. Vincent, C.S. Becquart, C. Domain, J. Nucl. Mater. 351 (2006) 88.
[40] E. Vincent, C.S. Becquart, C. Domain, J. Nucl. Mater. 359 (2006) 227.
[41] C. Domain, C.S. Becquart, J. Foct, Phys. Rev. B 69 (2004) 144112.
[42] P. Olsson, E. Vincent, C. Domain, in: Proceedings 'AES-ATEMA' 2007 International Conference (2007) 405.
[43] D. Kulikov, L. Malerba, M. Hou, Philos. Mag. 86 (2006) 141.
[44] C.C. Fu, Private communication within the PERFECT-project, (<www.fp6perfect.net>).
[45] K. Tapasa, A.V. Barashev, D.J. Bacon, Yu.N. Osetsky, J. Nucl. Mater. 361 (2007) 52.
[46] T. Tabata, H. Fujita, H. Ishii, K. Igaki, M. Isshiki, Scripta Metall. 15 (1981) 1317.
[47] A.V. Barashev, A.C. Arokiam, Philos. Mag. Lett. 86 (2006) 321.
[48] F.G. Djurabekova, L. Malerba, C. Domain, C.S. Becquart, Nucl. Instr. and Meth. B 255 (2007) 47.
[49] C.S. Becquart, C. Domain, J.C. Van Duysen, J.M. Raulot, J. Nucl. Mater. 294 (2001) 274.